



HAL
open science

Heat flux estimation in an infrared experimental furnace using an inverse method

P. Le Bideau, J.P. Ploteau, P. Glouannec

► To cite this version:

P. Le Bideau, J.P. Ploteau, P. Glouannec. Heat flux estimation in an infrared experimental furnace using an inverse method. *Applied Thermal Engineering*, 2009, 29 (14-15), pp.2977. 10.1016/j.applthermaleng.2009.03.014 . hal-00556853

HAL Id: hal-00556853

<https://hal.science/hal-00556853>

Submitted on 18 Jan 2011

HAL is a multi-disciplinary open access archive for the deposit and dissemination of scientific research documents, whether they are published or not. The documents may come from teaching and research institutions in France or abroad, or from public or private research centers.

L'archive ouverte pluridisciplinaire **HAL**, est destinée au dépôt et à la diffusion de documents scientifiques de niveau recherche, publiés ou non, émanant des établissements d'enseignement et de recherche français ou étrangers, des laboratoires publics ou privés.

Accepted Manuscript

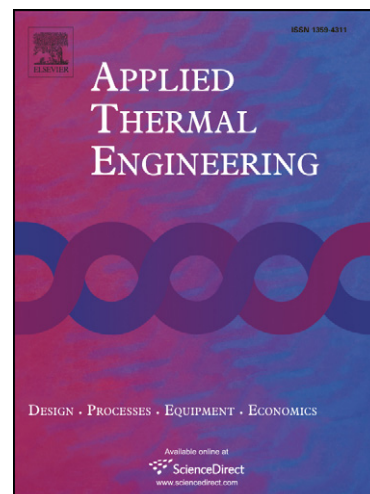
Heat flux estimation in an infrared experimental furnace using an inverse method

P. Le Bideau, J.P. Ploteau, P. Glouannec

PII: S1359-4311(09)00085-4
DOI: [10.1016/j.applthermaleng.2009.03.014](https://doi.org/10.1016/j.applthermaleng.2009.03.014)
Reference: ATE 2755

To appear in: *Applied Thermal Engineering*

Received Date: 23 May 2008
Accepted Date: 10 March 2009



Please cite this article as: P. Le Bideau, J.P. Ploteau, P. Glouannec, Heat flux estimation in an infrared experimental furnace using an inverse method, *Applied Thermal Engineering* (2009), doi: [10.1016/j.applthermaleng.2009.03.014](https://doi.org/10.1016/j.applthermaleng.2009.03.014)

This is a PDF file of an unedited manuscript that has been accepted for publication. As a service to our customers we are providing this early version of the manuscript. The manuscript will undergo copyediting, typesetting, and review of the resulting proof before it is published in its final form. Please note that during the production process errors may be discovered which could affect the content, and all legal disclaimers that apply to the journal pertain.

Heat flux estimation in an infrared experimental furnace using an inverse method

P. Le Bideau, J.P. Ploteau , P. Glouannec

Laboratoire LIMATB, Université de Bretagne Sud, Centre de recherche, Rue St Maude,

BP 92116, 56321 Lorient Cedex, France

Abstract

Infrared emitters are widely used in industrial furnaces for thermal treatment. In these processes, the knowledge of the incident heat flux on the surface of the product is a primary step to optimise the command emitters and for maintenance shift. For these reasons, it is necessary to develop autonomous flux meters that could provide an answer to these requirements. These sensors must give an in-line distribution of infrared irradiation in the tunnel furnace and must be able to measure high heat flux in severe thermal environments. In this paper we present a method for in-line assessments solving an inverse heat conduction problem. A metallic mass is instrumented by thermocouples and an inverse method allows the incident heat flux to be estimated. In the first part, attention is focused on a new design tool, which is a numerical code, for the evaluation of potential options during captor conception. In the second part we present the realisation and the test of this “indirect” flux meter and its associated inverse problem. “Direct” detectors based on thermoelectric devices are compared with this new flux meter in the same conditions in the same furnace. Results prove that this technique is a

reliable method, appropriate for high temperature ambiances. This technique can be applied to furnaces where the heat flux is inaccessible to “direct” measurements.

Keywords: Infrared radiation; Fluxmeter; Inverse heat conduction; Industrial furnace.

ACCEPTED MANUSCRIPT

Nomenclature**Symbol**

a	thermal diffusivity	$\text{m}^2 \text{s}^{-1}$
C	heat capacity	J K^{-1}
c_p	specific heat	$\text{J kg}^{-1} \text{K}^{-1}$
h	convection coefficient	$\text{W m}^{-2} \text{K}^{-1}$
k	thermal conductivity	$\text{W m}^{-1} \text{K}^{-1}$
q''	heat flux	W m^{-2}
S	surface	m^2
T	temperature	K

Greek symbols

α	absorptivity (radiation)	
ε	emissivity (radiation)	
ρ	density	kg m^{-3}
c	Stephan Boltzman	$\text{W m}^{-2} \text{K}^{-4}$

Subscripts

amb	ambient
cond	conduction
conv	convection
cor	correlation	
est	estimated
exp	experimental
fix	fixed
g	global

i	insulation
inc	incident IR radiation
m	metallic mass
rad	long wave radiation
w	wall

1. Introduction

Infrared radiation devices offer the possibility of providing high direct energy transfer to products. This heating mode enables energy to be transferred quickly and precisely to the material. For these reasons; it is widely used in transformation processes (drying, curing) [1-10]. To develop competitive processes, a perfect control of the IR irradiation is needed, which requires the knowledge of the incident heat flux received by the product. In theory, based on the spatial disposition of the infrared emitters and products, an irradiative balance could be performed to estimate the infrared radiation distribution inside the furnace and thus the heat flux received by the product. This approach can be complex because it requires knowing the characteristics of the heater, the age and wear of the heating plant must also be considered. Another solution is to measure directly the incident heat flux at the product surface using "in situ" sensors [11-14].

For many years our laboratory has been developing flux meters based on a semiconductor thermoelectric module which offers great sensitivity. In a previous study [14], we have put forth new conditions for these devices such as compactness, weak response time, and autonomy, as well as an easily measurable electrical output signal which directly correlates to IR irradiation. Nevertheless these "direct" flux meters are limited in autonomy and for very high heat flux densities.

This paper aims at presenting the feasibility of determining global high IR irradiation by the implementation of inverse analysis. The inverse problem has been an active area of research in heat transfer in the last few years [15-22]. In the present contribution the inverse heat conduction problem (IHCP) consists in estimating the time-variable incident heat flux on the surface of a material, knowing the temperature history (measurements) at a particular location in this material.

In the first part of this paper, the steps of the flux meter design are explained. Thus, a numerical study is carried out to proportion the material and to define the thermocouples positions. The temperature profiles used as input data for the IHCP are obtained from the solution of a direct 2D axisymmetric numerical model. This numerical study enables the validity of the 1D approach. A sensitive analysis of our problem is performed in order to quantify the error sources.

In a second part, the flux meter realization is described and experimental tests are carried out.

2. Fluxmeter design

The aim of this study is to determine the heat flux received by a product located in an infrared furnace. The infrared radiation is supposed to be isotropic and homogeneous at the product surface. The fluxmeter which can be exposed to high infrared radiation must endure to great thermal strains and it must have a sufficient thermal capacity to avoid great temperature variations during experimental tests. That is why, a metallic matter has been chosen. The metallic mass (cylindrical shape) is instrumented with temperature sensors and the whole is thermally isolated (bottom and lateral faces). In this configuration, only the surface is submitted to the incident infrared radiation, see Fig. 1.

The use of inverse methods entails previously performed numerical studies (sensitive analysis) to reach an optimal design that respects technical requirements. It is also necessary to study precisely the location of temperature sensors in order to reach a sufficient thermal sensitivity enabling heat flux identification.

A 2D axisymmetric numerical model was developed to represent the heat transfers inside the metallic mass and its insulation. Some simulations are performed with a fixed heat flux ($q''_{inc}{}^{fix}$) to study the influence of the geometry and the thermal properties of the mass (thermal capacity and thermal conductivity).

An inverse heat conduction problem using a 1D numerical model is also solved. It consists in the determination of the surface heat flux from transient temperature measurements in the solid. It uses an optimization approach. This program uses the temperature profiles previously generated by the 2D axisymmetric model and estimates the heat flux ($q''_{inc}{}^{est}$). This heat flux is compared with the heat flux fixed in the 2D axisymmetric model. The fluxmeter design is then modified: insulation and metal dimensions, thermal properties and thermocouple implantation. According to a typical design procedure [22], the problem is resolved until the difference between $q''_{inc}{}^{fix}$ and $q''_{inc}{}^{est}$ is minimized, see Fig. 2.

2.1 Presentation of the two-dimensional model

A 2D axisymmetric numerical model $T(r,z)$ is developed with the software Comsol®. We suppose the materials homogeneous and the thermo-physical properties constant. On the upper side of the metal and of the insulation an incident infrared radiation is imposed. During the sample heating, it exchanges heat with the environment by

convection and long-wave radiation, Fig. 1. At the lateral and bottom boundaries, only a convective exchange is imposed. So, the heat transfer equations are as follow:

$$0 < z < L \text{ and } 0 < r < R \quad (\rho c_p)_m \frac{\partial T_m}{\partial t} = k_m \left(\frac{\partial^2 T_m}{\partial z^2} + \frac{1}{r} \frac{\partial}{\partial r} \left(r \frac{\partial T_m}{\partial r} \right) \right) \quad (1)$$

$$0 < z < L' \text{ and } R < r < R' \quad (\rho c_p)_i \frac{\partial T_i}{\partial t} = k_i \left(\frac{\partial^2 T_i}{\partial z^2} + \frac{1}{r} \frac{\partial}{\partial r} \left(r \frac{\partial T_i}{\partial r} \right) \right) \quad (2)$$

Where the subscript m and i are respectively the metallic mass and the insulation

For the boundary conditions:

$$z = 0 \text{ and } 0 < r < R \quad -k_m \frac{\partial T_m}{\partial z} = q''_{conv,m} + q''_{rad,m} + \alpha_m q''_{inc}{}^{fix} \quad (3)$$

$$z = 0 \text{ and } R < r < R' \quad -k_i \frac{\partial T_i}{\partial z} = q''_{conv,i} + q''_{rad,i} + \alpha_i q''_{inc}{}^{fix} \quad (4)$$

Where α_m and α_i are the absorptivity of the metallic mass and insulation. The resolution is performed using a finite element method.

2.2 One-dimensional IHCP resolving

The problem consists in estimating the incident heat flux at $z = 0$ using the temperatures recorded at $z > 0$ (Fig. 1) and in considering only 1D conduction in the metallic material.

The governing equation is the following:

$$0 < z < L \quad (\rho c_p) \frac{\partial T}{\partial t} = k \left(\frac{\partial^2 T}{\partial z^2} \right) \quad (5)$$

And the boundary conditions are defined as follow:

$$z = 0 \quad -k \left(\frac{\partial T}{\partial z} \right)_0 = \alpha_m q''_{inc}{}^{est} + q''_{conv} + q''_{rad} \quad (6)$$

$$z=L \quad T(z,t) = T_{exp}(z,t) \quad (7)$$

The convective heat transfer is calculated with a free convection correlation for horizontal plate with the heated surface facing upward [15]:

$$q''_{conv} = h_{conv}(T_{amb} - T) \quad \text{with} \quad h_{conv}(T) = 1.32 \left(\frac{T - T_{amb}}{D} \right)^{0.25} \quad (8)$$

with D the flux meter diameter.

For the long wave radiation heat flux:

$$q''_{rad} = \frac{\varepsilon_m \sigma F (T_w^4 - T^4)}{(1 - \varepsilon_m) F + \varepsilon_m} \quad (9)$$

F represents the form factor between the emitter and the thermal mass surface. F equals 1 during the cooling period. Indeed, a radiant shield, which is supposed at the ambient temperature, is placed between the emitter and the metallic mass.

To solve the IHCP problem, the thermal evolution in two positions should at least be known. We suppose a first measurement at $z = d < L$. The second one is used for the boundary condition at the bottom ($z = L$).

To obtain acceptable sensibility, special attention to the first sensor location is needed [20, 21]. Indeed, to limit the amplification of noise measurements during the identification, deep implantation is chosen to respect the following criterion [20]:

$$1 > \Delta t_i > 10^{-2} \quad \text{with } \Delta t_i \text{ the characteristic time period: } \Delta t_i = \frac{a \Delta t}{d^2} \quad (10)$$

Δt is the temporal discretization in the numerical model.

Moreover, a time step Δt must be chosen, as the temperature evolution between two successive time steps is greater than the noise measurement T :

$$\frac{T(x_j, t + \Delta t) - T(x_j, t)}{\delta T} \gg 1 \quad (11)$$

The thermocouples should be accurately positioned in the metal to respect the following condition:

$$\frac{\delta x}{d} < 0,05 \text{ with } \delta x \text{ the thermocouple positioning error.} \quad (12)$$

The unknown heat flux is determined using an estimation algorithm which minimizes a quadratic criterion. This objective function equals the sum of squares of the differences between the measured and the computed temperatures at the selected spatial point:

$$S = \frac{1}{2} \sum_{t=1}^N (T(d, t) - T_{exp}(d, t))^2 \text{ with } N \text{ the number of measurements} \quad (13)$$

The estimation algorithm used in this study is the Levenberg-Marquardt algorithm [21].

2.3 Sensibility study and parameters influence

To study the sensibility of the method, we defined a typical incident IR heat flux which varies from 0 to 20 kW.m⁻² with a cyclic variation from 15 to 20 kW.m⁻² for 30 seconds. For practical purposes, these cyclic variations can correspond to the fluxmeter motion under four infrared heaters in a tunnel furnace. Ambient temperature is imposed at T_{amb}=30°C.

The influence of the thermal mass shape and thermal properties were first studied to choose the main design characteristics enabling the mono-dimensional hypothesis to be validated and the temperature sensor locations to be defined.

Next, a sensibilities study was performed to quantify the measurement uncertainty impact: noise measurement, sensor location errors, thermal properties.

2.3.1 Validation of the IHCP

The first simulation tests were performed to define the thermal characteristics of the metallic mass which must have a “low” thermal conductivity in order to obtain measurable temperature gradients in the mass. After several simulation tests carried out according to protocol, introduced in Figure 2, we obtained interesting results with thermal conductivity values equal to $20 \text{ W}\cdot\text{m}^{-1}\cdot\text{K}^{-1}$ and a thermal diffusivity equals to $5.1 \cdot 10^{-6} \text{ m}^2\cdot\text{s}^{-1}$.

To justify the use of a mono-dimensional approach, the temperature distributions according to the radius r were also studied.

In Figure 3, the temperature evolutions calculated by the 2D numerical model in the held metallic mass for different locations at $r = 0$ (surface, 2 mm and 4 mm under surface, bottom) and the incident heat flux are plotted.

Based on the first tests, we can note the thermal sensitivity is the greatest at the metallic mass surface. At this location, the temperature variations, caused by the cyclic variations of the incident heat flux, are distinctly visible. However, it is also more sensitive to environmental perturbations and the relative error in its location is great (cf. equation 12). To avoid this inconvenience and to respect the criteria defined earlier, we chose to place a thermocouple $d \approx 2.5 \text{ mm}$ under the surface. At this position, the sensor is sufficiently sensible to heat flux variations and considering a step time imposed at 0.5 s , we calculate a characteristic time equal to 0.31 s , i.e. $1 > \Delta t_i > 10^{-2}$.

The time constant of the thermocouple and the contact resistance between the sensor and the metallic mass are supposed negligible. Consequently, the necessary conditions enabling the IHCP convergence to be respected are verified (equations 10-11). Thus, as can be seen in Figure 4, the heat flux estimated ‘+’ is very similar to the fixed initial

heat flux (black line). The noted errors are mainly caused by the numerical approach (2D/1D model). These errors are weak except at the beginning and at the end of the radiation because of the great fixed heat flux variations. As great variations are not encounter in a real furnace. To test the method reliability, noise is added to numerical temperatures calculated by the 2D model:

$$T_{exp}(t) = T_{th}(t) + a \cdot \max(T_{th}(t)) \cdot \Delta \text{ with } a \in [-1, 1] \quad (14)$$

with T_{th} the calculated temperature from the 2D model. We add a white and normal noise where a is a random number, $\max(T_{th})$ the maximum temperature value and Δ is the magnitude of the perturbation. In the following numerical test Δ is taken to be equal 0.1 %. The noise data reaches 0.085 °C with these parameters. The impact of the noise data is presented in Figure 4. This one little disturbs the estimation of incident heat flux in comparison with the first test, which shows that a similar experimental noise is acceptable.

In the original test, the convection coefficient varies between 4 and 6 W.m⁻².K⁻¹ (cf. equation 8). To verify the impact of the lateral convection, this one is multiplied by 5. This parameter influence is weak, which shows the thermal mass is correctly dimensioned and insulated.

2.3.2 Influence of the thermo physical properties and thermocouple location.

Other errors caused by thermal properties of matter must also be considered. We suppose that the thermal properties (heat capacity, thermal conductivity) are measured with error equal to + 5 % and research is done to estimate the influence caused by these errors. Globally, we notice that the incident heat flux is overestimated but the relative mean error is weak and remains acceptable (Figure 5).

The error in the sensor location is also studied. Indeed, during the instrumentation step, it is difficult to place precisely a sensor inside a material. That is why it is important to determine this repercussion in the heat flux estimation. We suppose that the sensor is placed at 2.75 mm under the surface (instead of 2.5 mm).

For all these tests, the maximal relative error reaches 4.6% due to thermal mass capacity imprecision. Based on these results, we can conclude that the flux meter design seems to be satisfactory.

3. Experimentation

Following this sensibility study, the flux meter was manufactured and tested.

3.1 Flux meter realization

The material used is an inoxidable metal L316. Its thermal properties are very similar with the ones previously defined ($k = 16,3 \text{ W.m}^{-1}.\text{°C}^{-1}$, $\rho = 7960 \text{ kg.m}^{-3}$ $C_p = 500 \text{ J.kg}^{-1}.\text{°C}^{-1}$) and they are supposed constant in the studied temperature range ($T < 150\text{°C}$).

The cylindrical shaped block dimensions are 50 mm in diameter and 20 mm in height.

This block is placed in high temperature insulation (until 1100°C).

The irradiated surface is coated with a black graphite paint whose coefficients are

$\alpha_m = 0.9$ and $\varepsilon_m = 0.9$ in the field of medium and short infrared [15].

Three K-type thermocouples are embedded in the metallic mass. These sensors are manufactured with 75 μm diameter wire, i.e. a welding diameter equal to 250-300 μm .

For the exposed surface and the mass bottom, the sensors are positioned in surface notches and the welding is then crushed inside to obtain a good thermal contact. The time constant of the thermocouple is thus weak compared to the step time.

The surface sensor will be used to validate the simulated results in comparing the measured temperature with the calculated profile.

A third thermocouple is placed at 2.54 mm under exposed surface. A thin copper rod being used as an electrode was placed inside to ensure contact between the thermocouple and the metal during welding. This rod was then removed and the thermocouple position is known at 0.1 mm.

3.2 Experimental validation

The radiant heat source, used in these experiments, is equipped with three quartz tubes for a maximum of 6 kW emitting in short infrared range. The IR emitter power is modulated by a solid state relay operating in syncopated mode, which is piloted by a [0-10 V] input voltage. Tests are carried out in still air in natural convection. During the tests, the temperature evolutions for the three thermocouples and the ambience are recorded by a data acquisition system (10 acquisitions per second), see Fig. 6.

A radiative shield, at the room temperature, is placed between the emitter and the inert mass during the cooling periods.

Based on these measurements, the incident heat flux identification is performed with a step time imposed at 1 s, which is sufficient because the short-wave infrared emitters have a time constant superior to 1 s.

First, the global heat flux is estimated using the IHCP and the two measured temperatures (the bottom sensor and the embedded thermocouple). The global heat flux estimated and the simulated and experimental temperature differences are given in Figure. 7. To obtain this heat flux, the convective and radiative losses are removed from equation 6. Consequently, during the cooling period, the estimated heat flux equals

losses. So, knowing the losses, the surface temperature and the ambient temperature, a global heat coefficient is calculated for the different cooling periods (Table 1). As the surface, emissivity and the view factor between the mass and the environment are known, we can estimate the radiative losses. Therefore, the convective coefficient is deduced. The values of the convective coefficient are then compared with those calculated with the classical correlation (cf. equation 8) to validate the use of this correlation in the numerical model (cf. Table 1). We note a correct agreement between the experimental coefficient and the calculated convective coefficient.

In Figure 7, representing the simulated and experimental temperature differences, a weak difference is noticed ($<0.4^{\circ}\text{C}$).

Next, in introducing the losses in the thermal model, the estimated incident infrared irradiation is computed, see Fig. 8. During the cooling periods, the IR incident heat flux equals zero, which is in accordance with the expected results.

To validate the heat flux levels predicted by the IHCP, we compared, in the same conditions, the incident heat flux estimated by IHCP approach with the one measured with a “direct flux meter”. The latter is a non cooled detector using a semiconductor thermoelectric module [14].

In Figure 8, good agreement can be noted between the incident heat flux measured by the “direct” flux meter and the one estimated by IHCP. At the beginning of the test, when the infrared radiation is applied, the response obtained with the “direct” flux meter is longer. Indeed, this response difference is due to the thermal heat capacity of the thermoelectric module. We can notice the good fidelity for the two sensors.

3.3 Resolution study

An infrared irradiation corresponding to two input voltages, 8 V and 7.6 V, is applied as shown in Figure 9. For the IHCP solving, the step time is still 1 s. We noticed that the two flux meters are very sensitive to small heat flux variations: $\Delta q''_{\text{inc}} < 1 \text{ kW}\cdot\text{m}^{-2}$ which represents 5% of the heat flux. This high resolution is an important characteristic to detect a lamp dysfunction in an infrared tunnel.

Here again we observe a good agreement between the two heat flux sensors

3.4 High incident heat flux test

In furnace applications, high heat flux levels can be required. Then, we performed a test at the maximal power. The input signal (10 V) is applied. The thermal responses and the estimated incident heat flux are given in Figure 10.

The noise data is important, but reasonable for this heat flux level ($45 \text{ kW}\cdot\text{m}^{-2}$).

4 Conclusion

We developed a promising prototype for the characterization of infrared tunnel furnaces. The flux meters based on a thermoelectric module do not seem able to operate beyond $40 \text{ kW}\cdot\text{m}^{-2}$ incident flux. This new prototype has the advantage of being able to bear higher flux densities. The metallic mass and the two K type thermocouples located at 2.54 mm from the surface and at the bottom will never reach their functioning limits, thanks to the high heat capacity of the inoxidable mass. For the long times of exposition of the flux meter in industrial furnace, the temperatures can exceed 150°C . In this instance, the temperature dependent of the thermal properties should be taken into account in the numerical model.

This prototype is very sensitive to small heat flux variations which is an asset for an industrial application, for example evaluating the radiation homogeneity or detecting

lamp dysfunction in an infrared tunnel. It gives the “in-situ” incident or global irradiation of the treated product

In a future study, this flux meter will be test in a tunnel furnace in dynamic mode. This test will provide information concerning the flux meter resolution and its cut-off frequency.

References

- [1] V. Kosar, Z. Gomzi, Modeling of the power cable production line, *Thermochimica acta*, 457 (2007) 70-82
- [2] L. Véchet, I. Bombard, P. Laurent, J. Lieto, Experimental and modelling study of the radiative curing of a polyester-based coating, *International Journal of Thermal Sciences* 45 (2006) 86-93
- [3] P. Salagnac, P. Glouannec, D. Lecharpentier, Numerical modelling of heat and mass transfer in porous medium during combined hot air, infrared and microwaves drying, *International Journal of Heat and Mass Transfert* 47, N° 19-20 (2004) 4479-4489
- [4] P. Le Bideau, JP Ploteau, P. Dutournié, P. Glouannec, Experimental and modelling study of superficial elastomer vulcanization by short wave infrared radiation, *International Journal of thermal sciences* (2008) doi:10.1016/j.ijthermalsci.2008.03.016
- [5] N. Allanic, P. Salagnac, P. Glouannec, Convective and radiative drying of a polymer aqueous solution, *Heat and Mass Transfer* 43 (10) (2007) 1087-1095
- [6] J. Deans, M. Kögl, The curing of powder coatings using gaseous infrared heaters: an analytical model to assess the process thermal efficiency, *International Journal of Thermal Sciences* 39 (2000) 762-769

- [7] H. Lihan, Infrared surface pasteurisation of Turkey frankfurters, *Innovative Food Science and Emerging Technologies* 5 (3) (2004) 345-351.
- [8] F.M. Schmidt, Y. Le Maoult, S. Monteix, Modelling of infrared heating of thermoplastic sheet used in thermoforming process, *Journal of Materials Processing Technology* 143-144 (2003) 225-231.
- [9] R. M. Biefeld, A.A. Allerman, S.R. Kurtz, Recent advances in mid-infrared (3–6 μm) emitters, *Materials Science and Engineering B* 51 (1-3) (1998), 1-8.
- [10] D. Bauer, M. Heeger, M. Gebhard, W. Benecke, Design and fabrication of a thermal infrared emitter, *Sensors and Actuators A: Physical*, 55 (1) (1996) 57-63.
- [11] R. Bryant, C. Womeldorf, E. Johnsson, T. Ohlemiller, Radiative heat flux measurement uncertainty, *Fire and Material* 27 (2003) 209-222.
- [12] N. Martins, M.G. Carvalho, N. Afgan, A.I. Leontiev, A radiation and convection fluxmeter for high temperature applications, *Experimental Thermal and Fluid Science* 22 (2000) 165-173.
- [13] N. Arai, A. Matsunami, S.W. Churchill, A review of measurements of heat flux density applicable to the field of combustion, *Experimental thermal and fluid science* 12 (1996) 452-460.
- [14] J.P. Ploteau, P. Glouannec, H. Noel, Conception of thermoelectric flux meters for infrared radiations measurements in industrial furnaces, *Applied Thermal Engineering* 27 (2007) 674-681.
- [15] I.B. Fieldhouse, J.L. Lang, H.H. Blau, Investigation of feasibility of utilizing available heat resistant materials for hypersonic leading edge applications. Volume IV. Thermal properties of molybdenum alloy and graphite (1960) 1-78.

- [16] P. Wikstrom, W. Blasiak, F. Berntsson, Estimation of the transient surface temperature and heat flux of a steel slab using an inverse method *Applied Thermal Engineering* 27 (14) (2007) 2463-2472.
- [17] C.K. Chen, L.W. Wu, Y.T. Yang, Application of the inverse method to the estimation of heat flux and temperature on the external surface in laminar pipe *Applied Thermal Engineering* 26 (14) (2006) 1714-1724.
- [18] J.B. Baonga, H. Louahlia-Gualous, M. Imbert, Experimental study of the hydrodynamic and heat transfer of free liquid jet impinging a flat circular heated disk, *Applied Thermal Engineering* 26 (11) (2006) 1125-1138.
- [19] U.Z. Ijaz, A.K. Khambampati, M.C. Kim, S. Kim, K.Y. Kim, Estimation of time-dependent heat flux and measurement bias in two-dimensional inverse heat conduction problems, *Int. J. Heat and Mass Transfer* 50 (2007) 4117-4130.
- [20] M. Raynaud, Le problème inverse de conduction de la chaleur, *Techniques de l'ingénieur. Génie énergétique* 2 (1997) 1-17.
- [21] D. Marquardt, An Algorithm for Least-Squares Estimation of Nonlinear Parameters, *SIAM Journal Applied Math.* 11 (1963) 431-441.
- [22] Y. Jaluria, *Design and Optimization of Thermal Systems* 2nd edition, CRC Press, 2007.

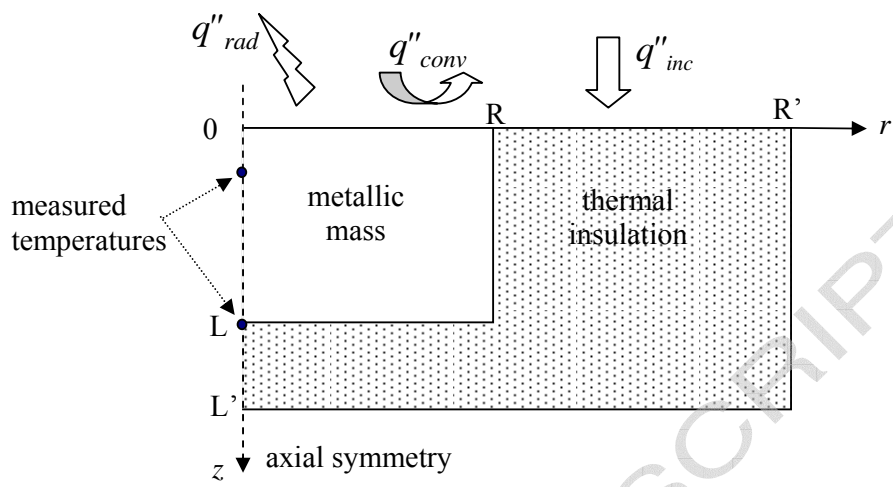


Fig. 1: Fluxmeter description

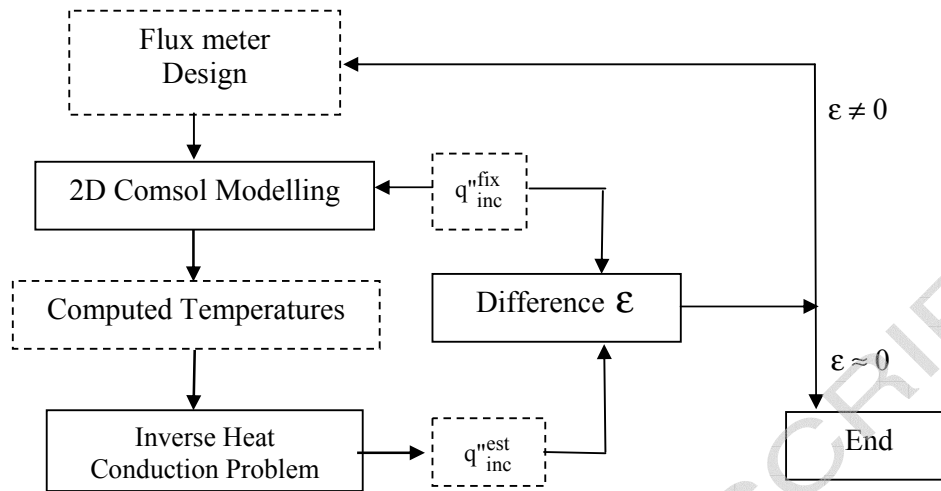


Fig. 2 Fluxmeter design methodology

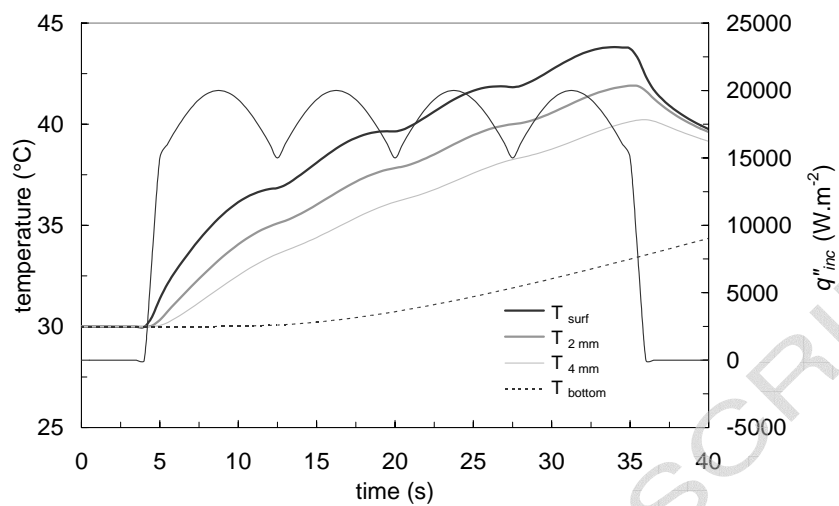


Fig. 3: Incident heat flux and computed temperature in the inoxidable mass (2D model).

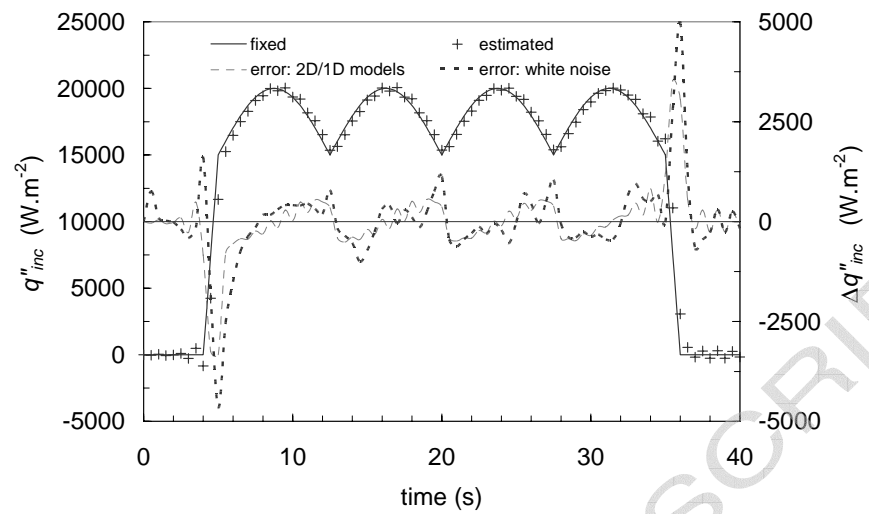


Fig. 4: Comparison between fixed and estimated heat flux from the 2D

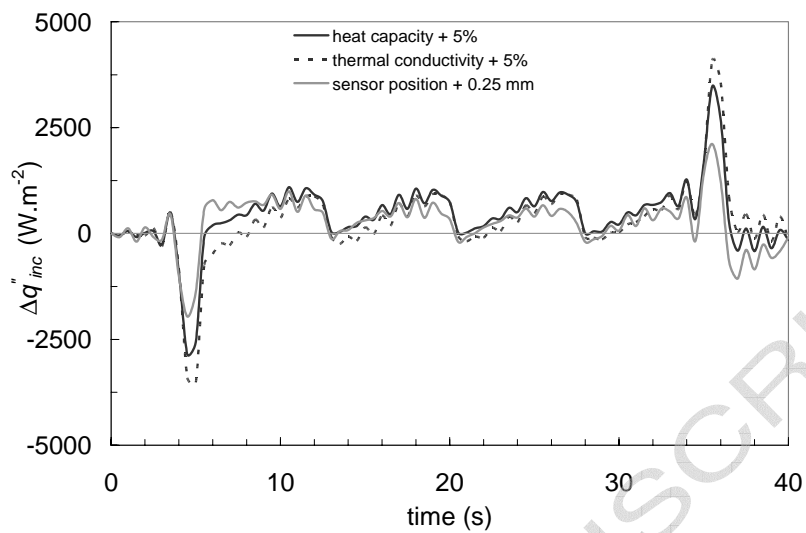


Fig. 5: Difference between the fixed and estimated heat flux
for perturbed temperature profiles

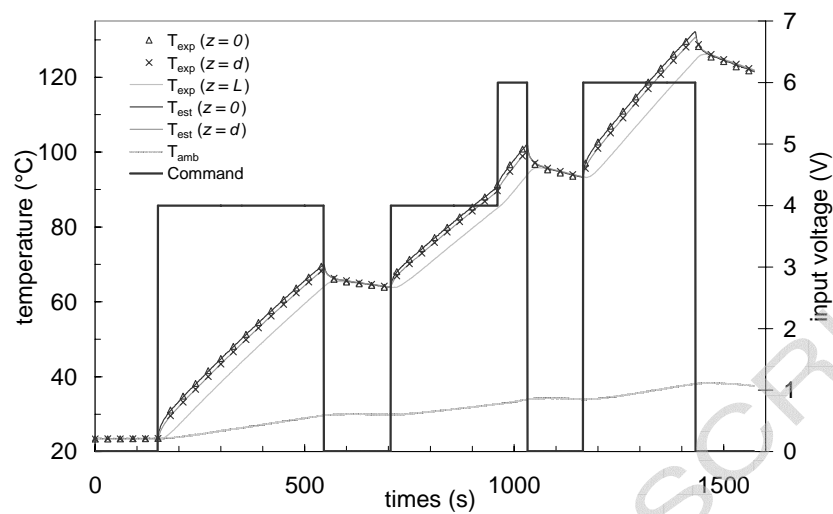


Fig. 6: Temperatures and input signal evolutions.

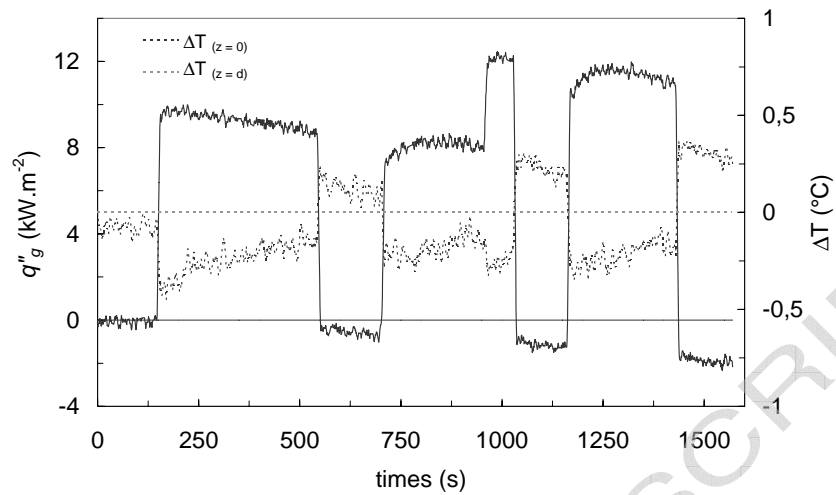


Fig. 7: Global incident heat flux identification and temperature difference between experimental and calculated data.

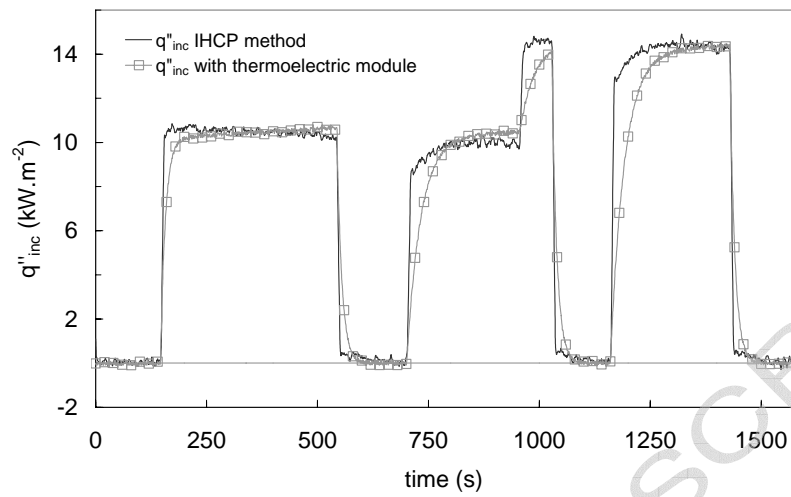


Fig. 8: Validation and fidelity study for direct and indirect sensors

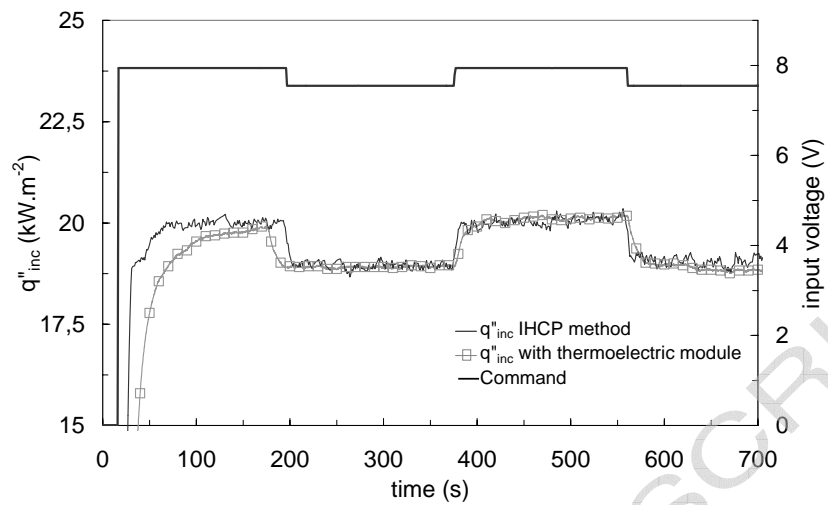


Fig. 9: Resolution study for direct and indirect sensors

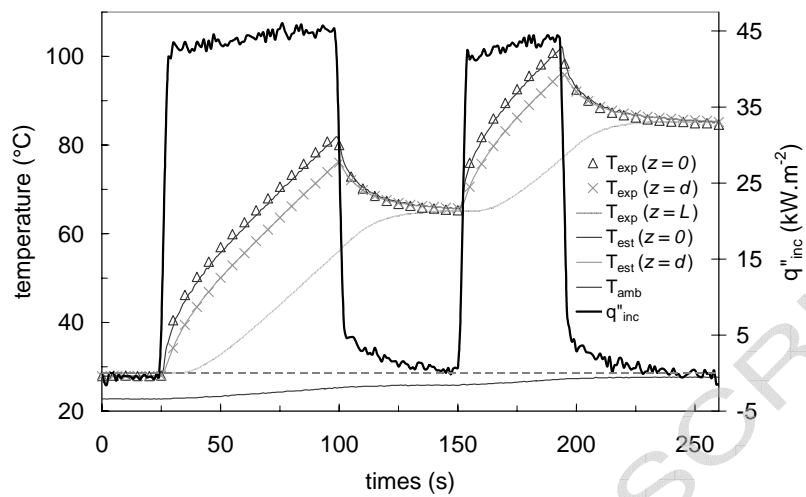


Fig. 10: IR incident heat flux and thermal responses.

Table 1: Comparison between calculated and estimated convective coefficient

	T_{surf} (°C)	T_{air} (°C)	$h_{g\ est}$ (W.m ⁻² .K ⁻¹)	$h_{conv\ est}$ (W.m ⁻² .K ⁻¹)	$h_{conv\ cor}$ (W.m ⁻² .K ⁻¹)
Cooling period 1	65.3	30.1	13.7	6.2	6.8
Cooling period 2	95.2	34.3	17.7	8.9	7.8
Cooling period 3	114.3	38.7	21.1	10.9	8.2